Deep-Sea Research I 92 (2014) 11–25

Contents lists available at ScienceDirect

Deep-Sea Research I

journal homepage: www.elsevier.com/locate/dsri

Biogeography and phenology of satellite-measured phytoplankton seasonality in the California current

Nicholas P. Foukal *, Andrew C. Thomas

School of Marine Sciences, Aubert Hall 360D, University of Maine, Orono, ME 04469, USA

ARTICLE INFO

Article history:
Received 16 December 2013
Received in revised form
5 June 2014
Accepted 15 June 2014
Available online 26 June 2014

Keywords:
Eastern boundary current
Phytoplankton
Remote sensing
Food webs, structure and dynamics
Chlorophyll
Clustering analysis

ABSTRACT

Thirteen years (1998–2010) of satellite-measured chlorophyll *a* are used to establish spatial patterns in climatological phytoplankton biomass seasonality across the California Current System (CCS) and its interannual variability. Multivariate clustering based on the shape of the local climatological seasonal cycle divides the study area into four groups: two with spring-summer maxima representing the northern and southern coastal upwelling zones, one with a summer minimum offshore in mid-latitudes and a fourth with very weak seasonality in between. Multivariate clustering on the seasonal cycles from all 13 years produces the same four seasonal cycle types and provides a view of the interannual variability in seasonal biogeography. Over the study period these seasonal cycles generally appear in similar locations as the climatological clusters. However, considerable interannual variability in the geography of the seasonal cycles is evident across the CCS, the most spatially extensive of which are associated with the 1997–1999 El Niño-Southern Oscillation (ENSO) signal and the 2005 delayed spring transition off the Oregon and northern and central California coasts. We quantify linear trends over the study period in the seasonal timing of the two seasonal cycles that represent the biologically productive coastal upwelling zones using four different metrics of phenology. In the northern upwelling region, the date of the spring maximum is delaying (1.34 days yr^{-1}) and the central tendency of the summer elevated chlorophyll period is advancing (0.63 days yr^{-1}). In the southern coastal upwelling region, both the initiation and cessation of the spring maximum are delaying (1.78 days yr^{-1} and 2.44 days yr^{-1}, respectively) and the peak is increasing in duration over the study period. Connections between observed interannual shifts in phytoplankton seasonality and physical forcing, expressed as either basin-scale climate signals or local forcing, show phytoplankton seasonality in the CCS to be influenced by changes in the seasonality of the wind mixing power offshore, coastal upwelling in the near-shore regions and basin-scale signals such as ENSO across the study area.

1. Introduction

The California Current System (CCS) forms the relatively cold and biologically productive eastern boundary of the North Pacific Gyre. Seasonal shifts in atmospheric pressure systems over the CCS are characterized by the Aleutian Low driving winter storms into the CCS with accompanying mean poleward alongshore wind stress. In summer, the North Pacific High blocks storms from the region and, coupled with the summer North American continental low, drives equatorward, alongshore winds (Bakun and Nelson, 1991; Checkley and Barth, 2009). These seasonal equatorward winds drive the surface Ekman layer of the ocean offshore, upwelling cold, nutrient-rich, subsurface water near the coast (Hill et al., 1998), and spurring elevated phytoplankton productivity that supports the highly productive marine ecosystem (Mann and Lazier, 2006). Latitudinal gradients in solar heating, light, and wind create a meridionally varying seasonal structure in both upwelling and phytoplankton concentrations (Hill et al., 1998; Thomas et al., 2001). Monthly mean winds are upwelling-favorable year-round south of ~33°N but become progressively more strongly seasonal and of increasing winter downwelling duration with increasing latitude (Bakun and Nelson, 1991). Superimposed on this seasonality is both strong interannual variability imposed by basin-scale, climate-related signals such as the El Niño-Southern Oscillation (ENSO) cycle (*e.g.* Kahru and Mitchell, 2000) and possible long-term trends such as increased upwelling from global warming (Bakun, 1990). While interannual anomalies (*e.g.* Thomas et al., 2003; Thomas and Brickley, 2006) and multi-year trends in phytoplankton biomass (*e.g.* Kahru et al., 2009; Thomas et al., 2013) are evident, the phytoplankton seasonal cycle itself remains less well understood in the CCS.

* Corresponding author. Present address: Duke University, Division of Earth and Ocean Sciences, 103 Old Chem, Box 90227, Durham, NC 27708, USA. Tel.: +1 919 681 8169.
E-mail address: Nicholas.Foukal@Duke.edu (N.P. Foukal).

http://dx.doi.org/10.1016/j.dsr.2014.06.008
0967-0637/

Accounting for about 65% of the overall signal in the CCS (Vantrepotte and Mélin, 2009), phytoplankton seasonality causes higher trophic levels such as zooplankton (Richardson, 2008), shrimps (Koeller et al., 2009), larval fish (Brander et al., 2001) and birds (Sydeman et al., 2006) to time aspects of their own seasonality to favorable periods of food abundance. Temporal changes within the seasonality (phenology) of phytoplankton biomass can therefore have large impacts on the ecosystem by disrupting trophic connections (Barth et al., 2007; Ji et al., 2010). Moreover, phytoplankton may be sensitive indicators of climate change (Taylor et al., 2002) and may be responsible for non-linearities in connections between physical forcing and ecosystem productivity (Kirby and Beaugrand, 2009; Di Lorenzo and Ohman, 2012).

Satellite ocean color data provide the only viable way to consistently and synoptically quantify the dynamic structure of phytoplankton biomass over large spatial areas. Satellites provide systematic coverage of seasonality across highly dynamic areas (Vantrepotte and Mélin, 2009). Although measurement of potentially subtle phytoplankton temporal changes is ideally made from platforms with high temporal resolution (*e.g.* moorings or gliders), previous work has demonstrated the feasibility of measuring phytoplankton phenology with satellite data both regionally and globally (*e.g.* Henson and Thomas, 2007; Racault et al., 2012).

Here we use 13 years of satellite-measured ocean color data to view phytoplankton seasonal biogeography over the entire CCS, quantify its interannual variability and document changes in phenology. We proceed in three steps: (1) identify the most dominant seasonal cycle shapes in the climatology and map their spatial pattern (climatological biogeography), (2) identify the same seasonal cycles shapes within each year and present interannual variability in their biogeography (interannual biogeography), and (3) analyze shifts in the timing of specific aspects of the annual cycle within the regions characterized by the dominant seasonal cycle shapes (phenology). Lastly, we briefly compare specific features of observed interannual changes in biogeography and phenology to both local and basin-scale physical forcing.

2. Background

2.1. Biogeography

Biogeography attempts to simplify biological patterns by defining regions of similar characteristics. For biological ocean data, chronic under-sampling of the ocean provides another incentive to defining regions: a mechanism to extrapolate relatively few measurements to a larger area (Longhurst, 2007). The advent of satellite-measured ocean color data products provided the means to quantify aspects of surface phytoplankton biogeography with high spatial resolution over global scales. Platt et al. (1991) divided the North Atlantic into 12 regions to estimate primary production. Longhurst (1995) divided the global ocean into over 50 biogeographic provinces based in part on phytoplankton seasonal cycles.

A difficulty with oceanic biogeography is the contrast between the dynamic environment and the static nature of boundaries. Phytoplankton biomass is known to be patchy at a wide range of spatial and temporal scales (Haury et al., 1978), indicating that very few individual organisms experience 'average' conditions (Mackas et al., 1985), and constraining the effectiveness of oceanic biogeography. Appropriate spatial scales for averaging are also both time and space dependent in the ocean (Denman and Abbott, 1988), and might vary with the goals of the biogeographical analysis (Denman and Powell, 1984). Biogeographic boundaries of the ocean are typically based on climatological conditions (*e.g.* Longhurst, 1995; Oliver and Irwin, 2008; D'Ortenzio and Ribera d'Alcalà, 2009; Vantrepotte and Mélin, 2009; Thomalla et al., 2011; D'Ortenzio et al., 2012) and thus do not necessarily reflect the environment at any single point in time. Fluid boundaries (*e.g.* Devred et al., 2007; Irwin and Oliver, 2009) alleviate this issue, though the timescales at which the maps should be redrawn raises other questions.

In the CCS (Fig. 1), biogeography has been widely used to simplify the highly dynamic environment. A survey of previous work suggests that the most common way of partitioning the CCS is latitudinally defined boundaries based on broad climatological hydrographic characteristics and obvious geographic features (*e.g.* Hickey, 1989). Studies defining three regions use borders at either Cape Blanco or Cape Mendocino and Point Conception (*e.g.* GLOBEC, 1991; Checkley and Barth, 2009; Kahru et al., 2009; Chenillat et al., 2012). Others use four regions, with divisions at the Oregon–California border or Oregon–Washington border, Cape Mendocino, Point Conception, and the U.S.–Mexico border or Punta Eugenia, (Longhurst, 1995; Kahru and Mitchell, 2001; Henson and Thomas, 2007). Ware and Thomson (2005) delineate five separate regions from Vancouver Island to Point Conception: Vancouver (47.5°N–50.5°N), Columbia (43°N–47.5°N), Eureka (40.5°N–43°N), Monterey (36°N–40.5°N) and Conception (32.5°N–36°N). Thomas and Strub (2001) use six regions, with boundaries at Juan de Fuca Strait, Cape Blanco, Cape Mendocino, Point Arenas, Point Conception, the U.S.–Mexico border, Punta Eugenia and Cabo San Lucas, leaving out the SCB and northern Baja California regions from their analysis. Henson and Thomas (2007) use multivariate clustering on satellite-measured phytoplankton pigment concentrations in the CCS to define alongshore-oriented biogeographical regions due to elevated levels in the coastal zone. Legaard and Thomas (2006) map the seasonal timing of the annual maxima and minima in satellite-measured phytoplankton pigment concentrations, showing similar alongshore oriented regions with a major discontinuity at Point Conception.

2.2. Phenology

Phenology is the study of the timing of periodic events in an organism's or population's seasonal cycle with respect to its environment. Phenology can reveal sensitive biological responses to climate change because temperature often cues the initiation and duration of life stages (Edwards and Richardson, 2004; Richardson, 2009). Warming temperatures cause many organisms to increase their metabolic rate, begin life history stages earlier, and progress through ontogeny more quickly (Walther et al., 2002; Parmesan, 2006; Yang and Rudolf, 2010). Some organisms respond more quickly than others to environmental cues (Ji et al., 2010), potentially creating temporal mismatches between trophic levels and severely impacting the ecosystem (Hjort, 1914; Cushing, 1990). As the base of the marine food web, phytoplankton biomass and the timing of events in its seasonal cycle are a critical control on the efficiency of carbon transfer to higher trophic levels, including economically important fisheries (Ware and Thomson, 2005; Platt and Sathyendranath, 2008).

Specific events that induced strong interannual variability in the CCS demonstrate how increased climate variability, a predicted outcome of global warming (IPCC, 2007), may influence this highly productive marine ecosystem (Schwing et al., 2006). There is evidence that many interannual events are linked to basin-scale climate signals. The El Niño event of 1997–1999 resulted in delayed and weak upwelling winds (Bograd et al., 2009) and an increased thickness of upper warm layers, reducing vertical nutrient flux and resulting in strong negative biomass anomalies (Kahru and Mitchell, 2000). The strong El Niño in 1983 brought similar hydrographic conditions (Thomas and Strub, 2001) as well as a decoupling of the spring arrival of upwelling winds and its

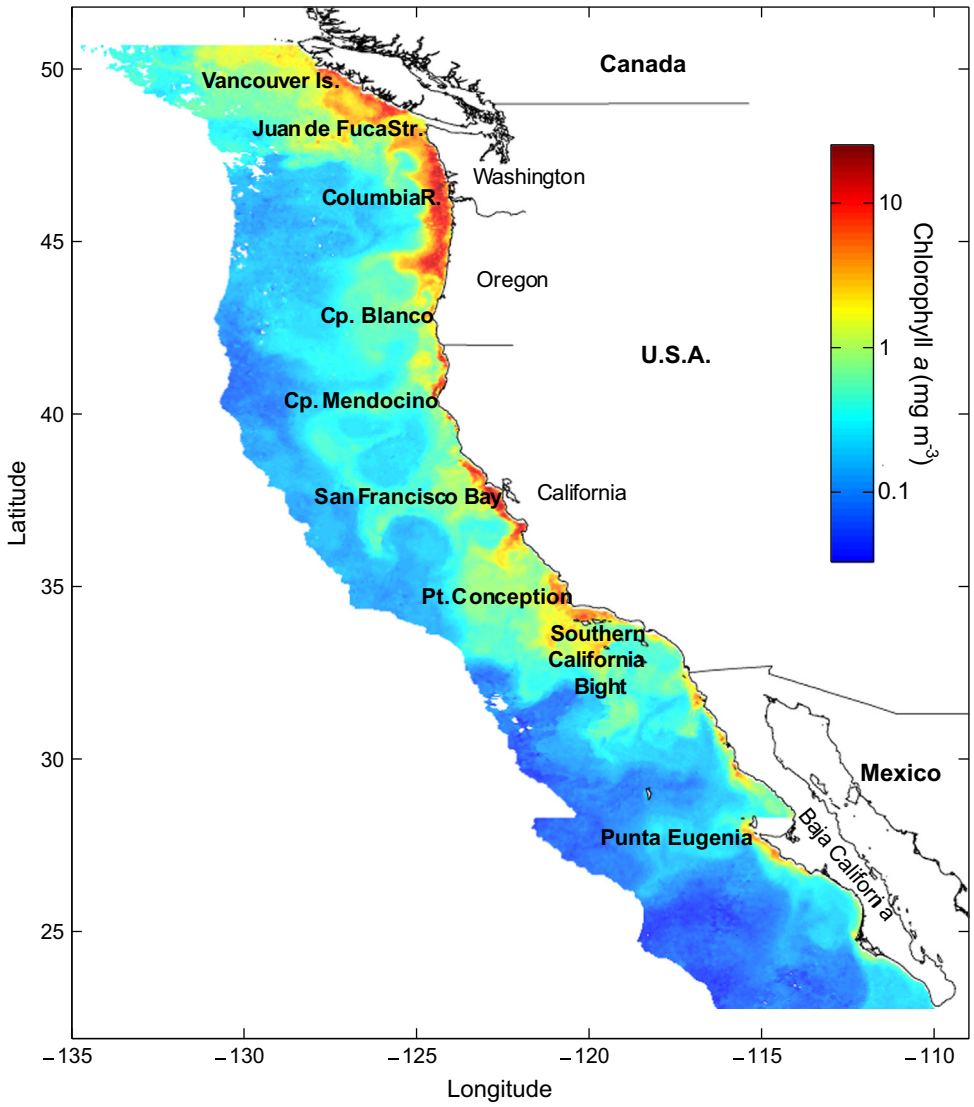

Fig. 1. Chlorophyll concentrations within the California Current study area in an example eight day composite of August 2010 from SeaWiFS satellite data. Relevant geographic locations and political boundaries are shown.

associated increase in phytoplankton biomass (Thomas and Strub, 1989). The latitude-dependent spring transition in the CCS from winter downwelling conditions to summer upwelling is the most prominent feature in the phytoplankton seasonal cycle (Strub et al., 1987; Kosro et al., 2006) and is controlled by seasonal changes in the large atmospheric pressure systems over the Pacific and western North America (Bane et al., 2007; Checkley and Barth, 2009; Black et al., 2011). A dramatically delayed arrival of spring upwelling winds in 2005 resulted in anomalously warm surface waters (Pierce et al., 2006), delayed phytoplankton blooms (Thomas and Brickley, 2006), population crashes of krill (Dorman et al., 2011) and reproductive failure of marine birds (Sydeman et al., 2006). This event provided clear evidence of the importance of upwelling timing to the structure of the ecosystem (Barth et al., 2007). There is evidence that the 2005 event had connections to the North Pacific Gyre Oscillation (Chenillat et al., 2012) and a southerly position of the jet stream (Bane et al., 2007).

In upwelling ecosystems, the anticipated trend in phytoplankton phenology due to global warming is unclear. Though climate-induced warming of sea-surface temperatures (SST) would imply weaker winters, earlier springs and later falls, phytoplankton respond most directly to light availability and nutrient flux, both of which are more closely linked to upwelling and wind mixing than temperature in an upwelling environment. Over the past four decades (1967–2007), the upwelling season, defined by alongshore wind forcing, shifted later and became shorter in the northern CCS while the upwelling season in the southern CCS became longer (Bograd et al., 2009). Thus the paradigm that warming SSTs on the global scale will result in poleward shifts and/or advances (delays) in the spring (fall) (Doney et al., 2012; Thomas et al., 2012a) may not apply in upwelling regimes.

Phytoplankton seasonality imposes a major control on the overall productivity of the CCS and provides a critical connection between physical changes in the environment, driven by local, basin-scale and/or global changes, and biological productivity. Quantifying phytoplankton seasonality spatially (biogeography) and temporally (phenology) provides insight into CCS ecosystem function, stability and susceptibility.

3. Data and methods

3.1. Study area

Our CCS study area extends from the northern edge of Vancouver Island (51°N) to the southern tip of Baja California (23°N),

and almost 700 km offshore (Fig. 1). This region encompasses the highly productive coastal upwelling regions of the CCS, the seasonally varying region seaward of this (Mackas, 2006; Thomas et al., 2012b) influenced by meanders in the coastal jet and eddies that are advected offshore from the coastal zones (Hill et al., 1998), and a portion of the offshore, more oligotrophic, subtropical/sub-arctic Pacific region (Yoder and Kennelly, 2003; Thomas et al., 2012b).

3.2. Chlorophyll data

Daily, 4 km, level 2 NASA SeaWiFS chlorophyll *a* (CHL) data with the standard band ratio algorithm (O'Reilly et al., 1998) and the most recent reprocessing (R2010) were obtained from the Ocean Biology Group at Goddard Space Flight Center (http://www.oceancolor.gsfc.nasa.gov). The standard NASA CHL algorithm performs well in the CCS (Kahru and Mitchell, 1999). We remapped all 13 years of data from 1998 through 2010 to a consistent projection over the CCS, though difficulties with the satellite in 2008, 2009 and 2010 produce discontinuities in the time series of up to four months. To fill gaps due to clouds, reduce variability, and produce a regularly sampled time series, we formed 8 day composites. Gaps in the 13 years of data longer than three composites (24 days) are filled with the climatology and shorter gaps are filled with temporal linear interpolation. The data are then smoothed temporally with a three period (24 day) running mean and spatially with a three-by-three pixel (12 km $\times$ 12 km) median filter to reduce high time and space frequency noise. Climatologies for each 8 day period are then formed from the median of the 13 years. Chlorophyll values in both the climatology and the 13 year time series are then log-transformed (Campbell, 1995) to further reduce the effect of episodic, isolated, high values, especially in coastal areas, and to better treat variability in both the high coastal values and lower offshore values together.

3.3. Multivariate clustering analysis

Multivariate clustering is used to identify the dominant seasonal cycle shapes in the CCS. We then map the spatial distribution of these seasonal cycles within our study area. Two separate clustering operations are performed with data from each location: (1) with the climatological seasonal cycle to identify the dominant seasonal cycle shapes, test the optimal number of clusters, and map the climatological spatial patterns, and (2) with the individual seasonal cycles from all 13 years to view the interannual variability of the seasonal cycle shapes identified in the climatology. In the latter clustering analysis, one single clustering operation divides all 13 years of data by treating the seasonal cycle of each year as an independent vector. Though the number of seasonal cycles passed into each of the two clustering operations is vastly different (13 $\times$ more in the interannual clustering), the pre-processing is identical. Prior to clustering, the seasonal cycle at each location and for every year is normalized to the annual mean to focus within-cluster similarity on the shape of the seasonal cycle, rather than differences in overall annual CHL magnitude. To retain differentiation of seasonal cycles of similar shape but differing amplitude, the seasonal cycles are not normalized to the seasonal maximum, as was done in a similar study (D'Ortenzio et al., 2012).

We then use the *k*-means multivariate clustering algorithm to group the locations according to the seasonal cycle shape, with the squared Euclidean distance as the metric of similarity and randomly selected cluster centroids as starting points. The *k*-means algorithm is an iterative process that maximizes the within cluster similarity without requiring prior knowledge of where the clusters are (spatially) or the shape of the cluster centroids (the characteristic phytoplankton seasonal cycle). The *k*-means algorithm requires specification of *k*, the number of clusters to produce, which we identify in the climatology. The appropriate number of clusters is inherently subjective (Pielou, 1977, 1984; Manly, 2004), though there are statistical tests that can guide the user. One commonly used tool in *k*-means is silhouette analysis (Rousseeuw, 1987), which calculates for each pixel the normalized difference between the distance to the centroid of its assigned cluster and the distance to the next closest cluster centroid to which it was not assigned. Thus the average silhouette value can provide an indication of the optimal number of clusters within a data set. However, silhouette maps from our climatological data set with *k* varying from two through ten show the average silhouette width across the study area to be highly sensitive to the length of the boundary where two or more seasonal cycles border; regardless of the suitability of the clustering, results with large border regions have low (poor) average silhouette widths, whereas results with small border regions have high (good) average silhouette widths. Thus we chose other selection criteria to decide on an ideal *k*.

With the primary goal of determining the dominant phytoplankton seasonal cycle shapes across the CCS, we note that increasing *k* (starting from two) in the climatology produces unique seasonal cycle shapes until *k* equals four. Thereafter, further increases in *k* yield seasonal cycles that closely resemble one or more previously defined shapes. Results using two clusters separate the coastal upwelling zone from the offshore region, but provide little biogeographical insight and no description of the latitudinally-varying seasonality shown in previous studies (*e.g.* Legaard and Thomas, 2006). With *k* equal to three, tests on the reproducibility of the clusters from multiple runs on the climatology are unstable, indicating sensitivity to the initial, randomly assigned, centroid values. The results switch between two possible cluster combinations: one with a single offshore region and two coastal upwelling zones; and another with a single coastal upwelling region, a transition region and an offshore zone. Results from multiple runs of *k* equal to four produce stable, relatively unique and distinguishable clusters (consisting of the two possible combinations of three clusters). As an additional test, a hierarchical clustering algorithm is used on a spatially sub-sampled (factor of 10) version of the climatology. Although impractical to apply to large data sets, these algorithms do not require specification of the number of clusters (*k*), and show branch points as a function of distance. The dendrogram produced by this test (not shown) indicates that the branch points for three and four clusters are very close in distance; thus increasing *k* from three to four provides additional information while maintaining similar distances between the cluster centroids. Although the potential for bias due to the sub-sampling cannot be discounted, these results provide an additional test of the suitability of using four clusters in the *k*-means algorithm. We also examine sensitivity of the four climatological cluster seasonal cycle shapes to changes in our offshore boundary. Tests demonstrate that shapes were robust to removal of the offshore 100 km and 200 km of the study area. The combination of these results suggests that four clusters reasonably summarize the dominant seasonal cycle shapes across the CCS.

We then examine the interannual variability in the geography of these four seasonal cycle shapes by applying *k*-means clustering to the 13 year data set, where each year enters the clustering as a separate vector. The goal of this clustering operation was to find and track the same four seasonal cycle shapes identified in the climatology over the study period. Varying *k* in this larger data set showed similar characteristic seasonal cycles to the corresponding runs with the climatology. With *k* equal to four, the cluster means from the 13 year data set were almost identical to those identified in the climatology. Tests on the reproducibility of this interannual clustering showed that the four clusters were stable over multiple runs. We also tested the suitability of the grouping with a

hierarchical clustering algorithm on a spatially sub-sampled (factor of 100) version of the 13 year data set, with very similar results (not shown) to those of the climatology. Branch points in this dendrogram between three and four clusters were very close, and these were distinct from the many lower branches. Again, the possibility of biases created by subsampling cannot be ruled out, but these results provide an indication of the suitability of the four clusters in the interannual clustering.

3.4. Surface wind data

Wind data are daily, 1/4 degree, 10 m wind vectors over the study area from the NOAA Blended Sea Winds product (http://www.ncdc.noaa.gov). Data from 1998 to 2010, concurrent with the CHL time series, are products of no fewer than four satellite scatterometers (Zhang et al., 2006). Wind stresses in the x and y directions as well as wind mixing power (characterized as U^{*3}) are then calculated from the individual daily vectors using the drag coefficients of Yelland and Taylor (1996). Coastal upwelling, or cross shelf mass transport ($m^3\ s^{-1}$) per 100 m of coastline, is quantified at every 1° latitude interval along the coast using the local ($\pm 0.5^\circ$ latitude) orientation of the coastline and the local Coriolis parameter. The wind stresses, U^{*3}, and coastal upwelling transport are then averaged into 8 day periods to match the CHL data.

3.5. Phenology

Many metrics of CHL phenology exist. These include the date of the annual maximum (Yoo et al., 2008; Kahru et al., 2011), the central tendency (Edwards and Richardson, 2004), the maximum rate of change of CHL prior to a peak (Brody et al., 2013), the timing and duration of CHL greater than 5% above the annual mean (Siegal et al., 2002; Henson et al., 2006; Henson and Thomas, 2007) or above a particular threshold concentration (Okamoto et al., 2010), the date that the running sum reaches a certain percentage of the annual total (Greve et al., 2005; Brody et al., 2013), the inflection point on a curve-fitted time series (Koeller et al., 2009), and the number of weeks after February 1 that CHL first exceeds 20% of the annual maximum (Fuentes-Yaco et al., 2007). Holt and Mantua (2009) examine many different metrics of the physical spring transition in the CCS and find that due to different hydrographic properties, different latitudes warrant different metrics. Bograd et al. (2009) develop a series of upwelling phenology metrics based on the cumulative sum of upwelling intensity in the CCS that provide insight into shifts of upwelling seasonality. Our results from the clustering analysis on the climatology suggest that the same CHL phenology metrics would not be equally effective in each region of the CCS. Here we use four metrics of phytoplankton phenology. The date of the spring maximum isolates a single date when CHL is at its maximum level between January 1 and May 30. The summer central tendency characterizes the date of the center of mass over the time period June 1–December 31, summarizing biomass shifts over a larger time domain. The bloom begin and end dates are the first and last dates of the longest consecutive time period above the annual mean in each year and thus capture the timing and duration of the longest bloom of the year. We then view the interannual variability in these metrics and calculate their slope (trend) over the 13-year study period.

Estimation of the significance levels to the least squares fit slopes of the phenology metrics requires estimation of n, the number of independent realizations in each year. Spatial autocorrelation within the CHL data and reflected in the phenology values in each year means that each location cannot be considered independent. We estimate n by calculating example spatial decorrelation scales in each of the alongshore and cross-shelf directions within each biogeographic region for which we calculate a phenology metric. Alongshore decorrelation scales range from 11 to 17 pixels (44–68 km) and cross-shelf decorrelation scale range from 7 to 10 pixels (28–40 km) among the phenology metrics. For each metric, we then divide the total number of locations (pixels) in each region by the product of the two to provide an estimate of n. An analysis of variance that results in an

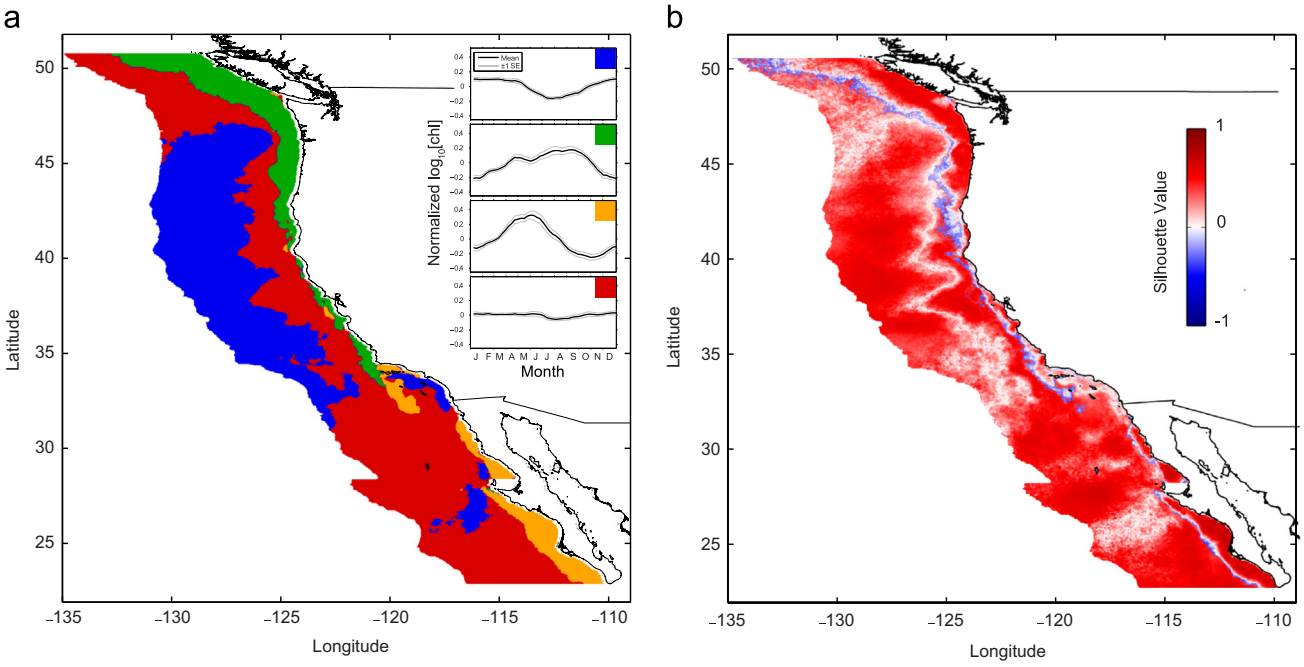

Fig. 2. The four seasonal cycle shapes from the climatological clustering. (a) Mean phytoplankton seasonal cycles and standard errors within the four climatological cluster groups (top right) and their spatial geography in the study area. (b) Silhouette values across the study area indicate similarity to their respective cluster centroid. Low silhouette values occur near the boundaries, indicative of gradual transitions. (For interpretation of the references to color in this figure legend, the reader is referred to the web version of this article.)

F value with 1 and $n-2$ degrees of freedom applied to the linear model tests the null hypothesis that the regression slope is zero for the case of multiple observations at each time step (Sokal and Rohlf, 1995). Phenology metrics in different years are assumed to be independent.

4. Results

4.1. Climatological biogeography

Cluster analysis of the climatological seasonality in satellite-measured CHL suggests that the CCS can be partitioned into four dominant phytoplankton seasonal cycles (Fig. 2a). These map to an offshore region, two coastal regions (northern and southern) and a transition region between them. A distinct summer CHL minimum (July–October) and elevated levels in winter, spring and late fall define the offshore region (blue, ~30% of study area). Hereafter, we refer to this seasonal cycle as 'Summer Min'. Geographically, this seasonal cycle occurs in the offshore regions of the study area between 30°N and 45°N, as well as smaller regions offshore of Punta Eugenia and in the Southern California Bight (SCB).

The seasonal cycle characterized by a spring peak in April and May, then a longer, late summer elevated period from July through October maps to the northerly coastal region (green, ~20% of study area). We refer to it as the 'Late Peak' seasonal cycle. Geographically, it encompasses most of the coastal zone off Vancouver Island, Washington, Oregon and northern and central California, extending as far as 600 km west of the coast in the north, and decreasing in width until just south of Point Conception where it disappears.

An early season peak, with CHL increasing from November through May and decreasing from its peak in early June to a minimum in late October, defines the southerly coastal region (orange, ~10% of study area). We label this seasonal cycle 'Early Peak'. Its primary location is off Baja California and in the SCB, although small regions also appear off San Francisco Bay, Cape Mendocino and outside Juan de Fuca Strait.

Weak seasonality characterizes the last region (red), thus we name it the 'Flat' seasonal cycle. It is the largest (~40% of study area), is present over the entire range of latitudes examined here, and is broadest at latitudes south of ~33°N. It maps to a transition region between ~30°N and 45°N, but extends from the coastal region to the western edge of our study area at latitudes greater than and less than this range.

The most heterogeneous region is the SCB where all four climatological seasonal cycles are present. The Summer Min seasonal cycle appears in the near-shore region of the SCB, the Late Peak seasonal cycle extends southward beyond Point Conception, the Early Peak seasonal cycle appears in the northern coastal and southern offshore sections of the SCB, and the Flat seasonal cycle appears in the middle. The presence of all four seasonal cycles in this relatively small region points to the small-scale spatial diversity of conditions in the SCB, unique in comparison to other regions of our study area.

The silhouette values across the study area (Fig. 2b) show that much of the study area clusters closely to their respective centroids (red regions). However, there is strong spatial autocorrelation in the original data and pixels in boundary regions often group weakly to their centroid. Our biogeographic boundaries are not meant to imply step-like shifts from one cluster to another but rather a transition in similarity that is objectively quantified by the distance metric and the k-means algorithm. Areas that cluster less strongly to their centroid include the borders between the transition and offshore regions, the offshore region north of 45°N and directly west of Point Conception, the SCB, and an area southwest of Punta Eugenia. Negative (blue) silhouette values indicate assignment errors remaining when the iterative k-means algorithm stabilizes and stops. This occurs primarily at the boundary between the strongly differing seasonality of the coastal upwelling region and the offshore region.

4.2. Interannual biogeography

Multivariate clustering of the 13-year data set provides a view of the extent to which the climatological patterns in space are stable (Fig. 3). Specifying four clusters results in similar seasonal cycle shapes to those from the climatological clustering (Fig. 2a). Minor differences between the means of the climatology and those in Fig. 3 include a flatter elevated period in the Late Peak (green)

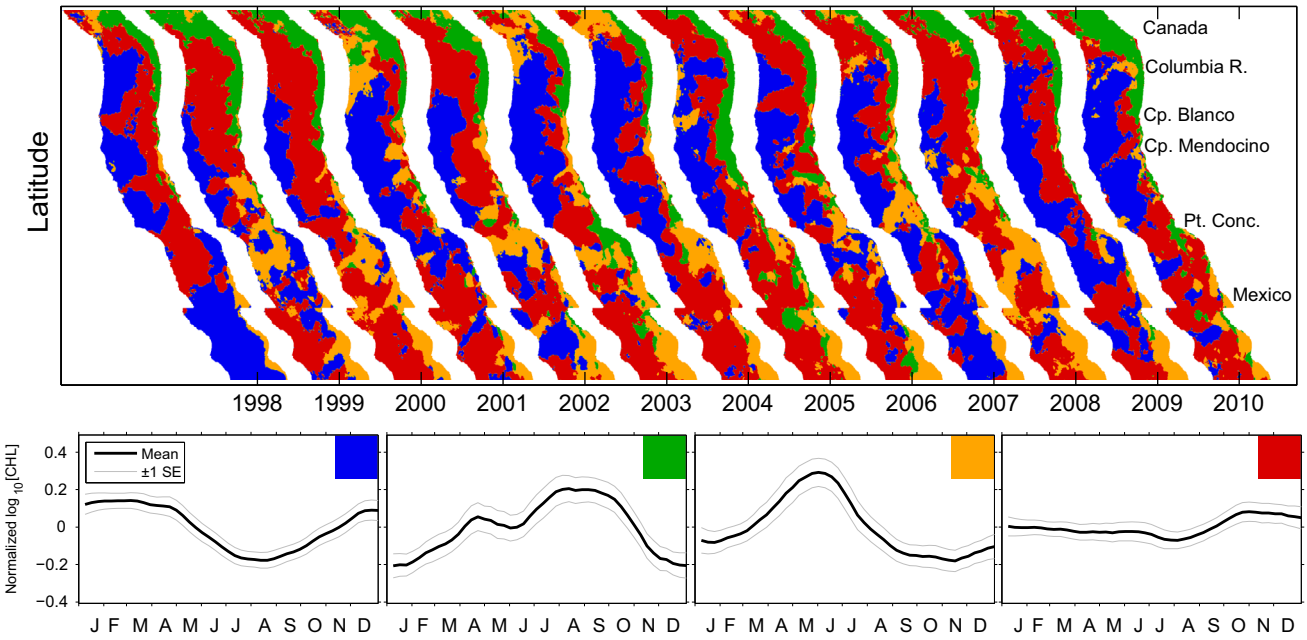

Fig. 3. Mean phytoplankton seasonal cycles and standard errors within the four cluster groups defined by the individual annual cycles (bottom) and their spatial geography within the study area in each year. (For interpretation of the references to color in this figure legend, the reader is referred to the web version of this article.)

seasonality, a flatter autumn period in the Early Peak (orange) seasonality and a higher late autumn period in the Flat (red) seasonality. Variances within each of the seasonal cycle clusters are also larger in the interannual clustering than in the climatological seasonal cycles due to the larger number of entries into the clustering that are averaged over in the climatology.

The overall spatial geography of the seasonal cycles is relatively consistent from year to year. The Summer Min seasonal cycle is usually offshore, the Late Peak seasonal cycle is generally associated with northern coastal areas (Vancouver Island, Washington, Oregon and northern California), the Early Peak seasonal cycle is typically off Baja California, and the Flat seasonal cycle separates the coastal areas from the Summer Min seasonal cycle. Superimposed on this broad-scale consistency, however, is strong interannual variability in the spatial structure; in any given year, shifts in the biogeography occur. On average, 46% of the study area is assigned a different cluster than the previous year, with a maximum of 57% shifting between 1998 and 1999, and a minimum of 39% shifting between 1999 and 2000. In particular, some years in the CCS appear to experience an expansion of the Summer Min seasonal cycle (1998, 2001, 2007 and 2009), and in other years an expansion of the Early and Late Peak seasonal cycles and an offshore extension of the Flat seasonal cycle (1999, 2000 and 2008). Comparison of years 2008, 2009 and 2010 to others requires caution as data gaps required portions of the seasonal cycle to be filled with the local climatology (explained in Section 3.2).

Other features evident in the interannual variability of biogeography include a reduced area occupied by the Late Peak seasonal group in 1998 and a strong southward expansion of this group in 2005. The only year that the SCB is characterized as Late Peak is 2003. The Early Peak group is reduced in 1998 and 2010 even off Baja California, but occupies relatively large regions along the California coast in 1999, 2000, 2007 and 2008. In 1998, 2002, and 2007, large areas at the southern-most latitudes are dominated by the Summer Min seasonal cycle but this seasonal cycle occupies small areas over the whole study area in 2000 and 2008.

One way to summarize Fig. 3 is to show the interannual variability in the geographic area covered by each seasonal cycle (Fig. 4). The decline in the geographic area of the Summer Min (blue) seasonal cycle in our study area from 1998 to 2000 is evident. Most of this area is replaced by the Flat seasonal cycle (red), but a rebound of the coastal seasonal cycles, Early Peak and Late Peak in 1999 is also evident. The increase in size of the Late Peak (green) seasonal cycle in 2005 associated with the delayed upwelling season of that year is also noticeable.

Another way to summarize the interannual variability in Fig. 3 is to quantify those locations consistently in the same seasonal cluster, and those that often shift from one cluster to another. The Simpson Diversity Index (Simpson, 1949) provides a metric of both the number of changes and how diverse the changes are, valuing how many different seasonal cycle shapes a given location experiences over the 13 years (Fig. 5). Not surprisingly, areas near the geographic centers of the climatological regions are relatively stable over the study period. These regions include the coastal zones off Vancouver Island, Washington, and Oregon, the farthest offshore regions off northern and central California, and the Baja California coastal zone. Strong interannual seasonal diversity is present over most of the coastal region from Cape Blanco south to ~30°N, including the SCB, and regions west.

4.3. Phenology

We focus on the two coastal seasonal cycles that represent the biologically productive upwelling region, Late Peak and Early Peak, to examine aspects of phenology. The Flat seasonal cycle is not conducive to examination of phenology and the Summer Min seasonal cycle represents a small portion of the much larger North Pacific basin, changes over which are most appropriately investigated using data encompassing the entire North Pacific.

The interannual seasonal clusters (Fig. 3) are used to examine phenology, thus tracking changes within seasonal cycle types in the CCS rather than the phenology of any specific fixed geographic location. We quantified the phenology within the seasonal cycles by applying metrics of phenology suitable to the seasonal cycle shape to be examined; interannual variability (Fig. 3) suggests that in many locations, a single metric of phenology may not be applicable in all years. However, observed shifts in the phenology need to be interpreted in the context of possible changes in the spatial extent and/or the location of the cluster. Here we seek systematic shifts in phenology over the study period. Visual inspection of Fig. 3 suggests that no discernible systematic trends in the spatial structure of the biogeographic provinces are evident over the study period. In addition, examination of the annual means of both the seasonal cycle latitudes and their cross-shelf distances showed no systematic trends over the study period. This suggests that any observed study period trends in the phenology of the seasonal cycles within the two coastal seasonal cycles are not unduly biased by spatial shifts. However, episodic shifts in the phenology from one year to another do need to be compared to the biogeographic maps because the changes in timing may be linked to shifts in space.

Spatially-averaged seasonal cycles in each year of the two coastal regions from Fig. 3 are shown in Fig. 6 as heat-maps and compared to the climatological seasonal cycle. Shifts in phenology are evident. In the Late Peak group (Fig. 6a), the spring bloom occurs in late March and early April from 1998 to 2000 but then breaks into two

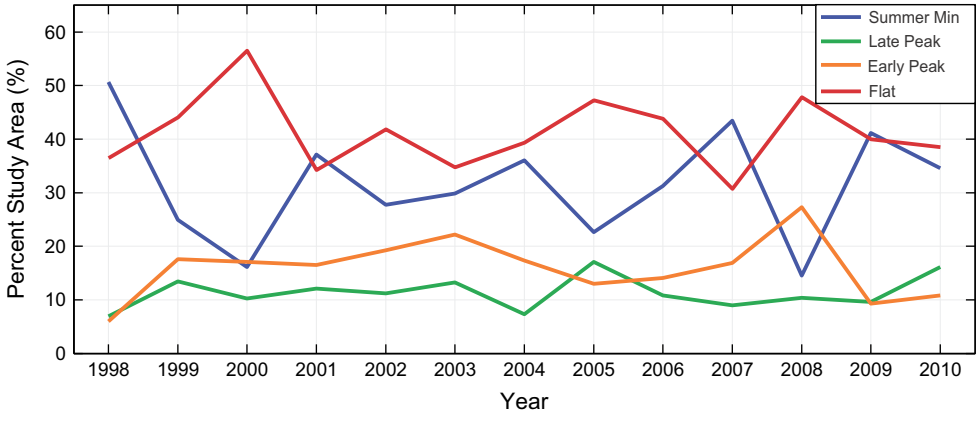

Fig. 4. Interannual variability in the geographic area of each seasonal cycle as a percent of the study area. (For interpretation of the references to color in this figure legend, the reader is referred to the web version of this article.)

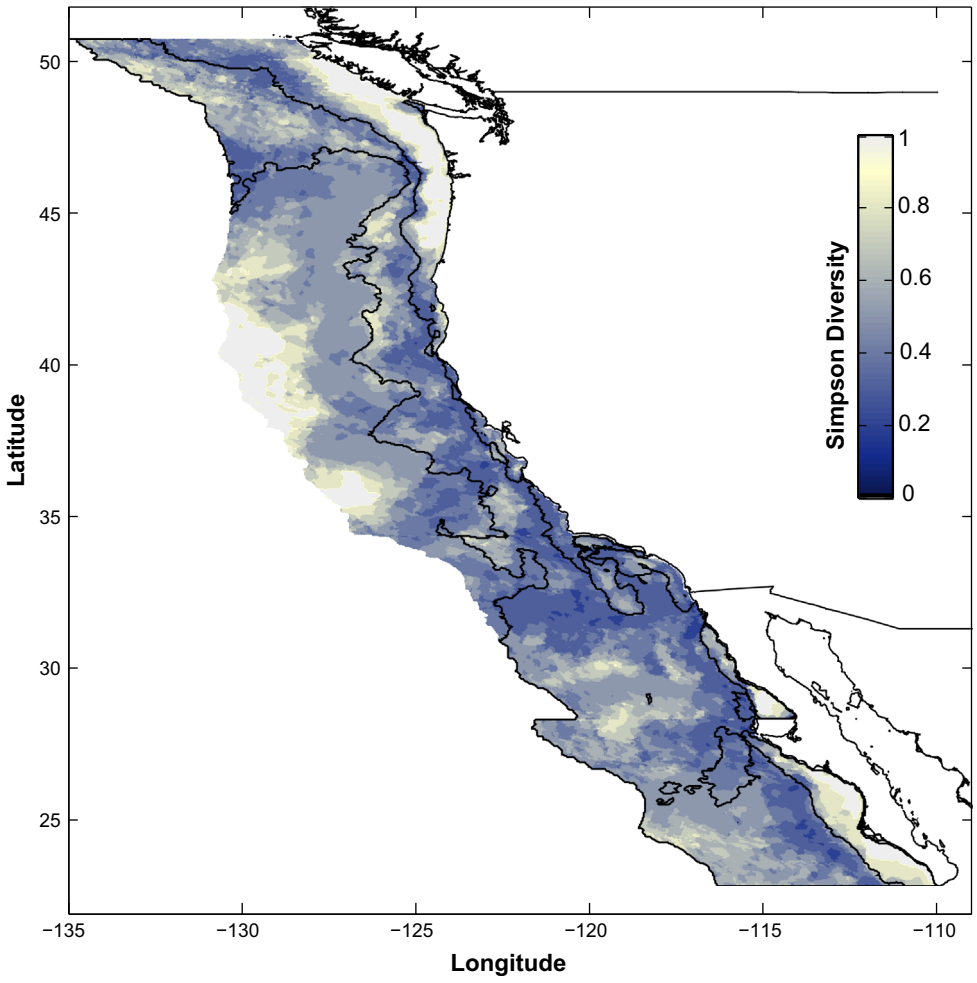

Fig. 5. Interannual stability of phytoplankton seasonality over the 13 year study period as measured by the Simpson Diversity Index. Larger values indicate more stability. Borders of the climatological biogeography are shown in black for reference.

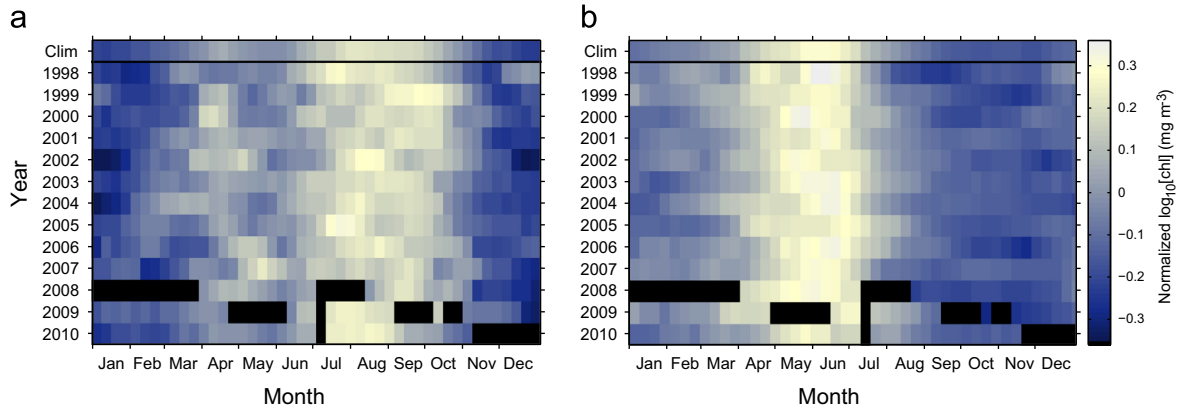

Fig. 6. Heat-maps of interannual variability in seasonal CHL concentration within the spatially-averaged Late Peak (a) and Early Peak (b) seasonal clusters from Fig. 3. The climatological seasonal cycle for each cluster type is displayed on the top row. Data are normalized to the annual mean to compare the relative timing rather than the absolute magnitudes of the seasonal cycles. Black indicates periods of missing data.

(most obvious in 2005 and 2006), or sometimes three (*e.g.* 2007) distinct peaks. From 2004 through 2007, there appears to be a bifurcation, with a smaller early spring bloom occurring progressively earlier and a larger, later, spring bloom occurring later in each year. The timing of the elevated summer period also exhibits interannual variability: early in 1998 and 2004 and late in 1999 and 2007. In the Early Peak group (Fig. 6b), interannual variability in the timing of the annual peak shows early years in 1999 and 2004, and late years in 1998 and 2003. Overall, however, the seasonal cycle of the Early Peak group appears more consistent interannually than that of the Late Peak group. In addition, the end of the seasonal peak appears to be more interannually stable than the initiation.

The dates of two phenology metrics for each of these coastal groups are presented in Figs. 7 and 8. Each suggests progressive but relatively small shifts in timing over the study period. In the Late Peak group (Fig. 7), the seasonal cycle was divided into two

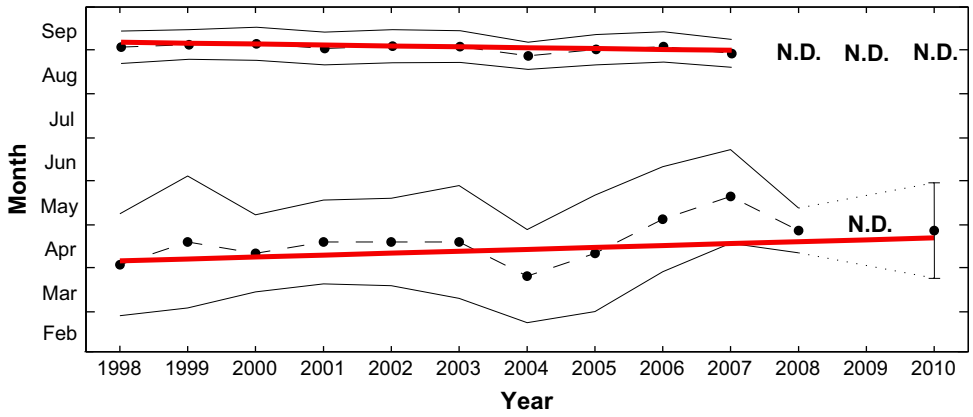

Fig. 7. The phenology of two metrics of the Late Peak seasonal cycle over the study period. Data are medians (black circles), ±1 standard deviation (thin lines) and the least squares fit linear trend (red lines). The summer central tendency (a) is advancing at 0.63 days yr^{-1} and the date of the spring maximum (b) is delaying at 1.34 days yr^{-1}. Missing data in 2008, 2009 and 2010 prevented calculation of one or both of these phenology metrics. (For interpretation of the references to color in this figure legend, the reader is referred to the web version of this article.)

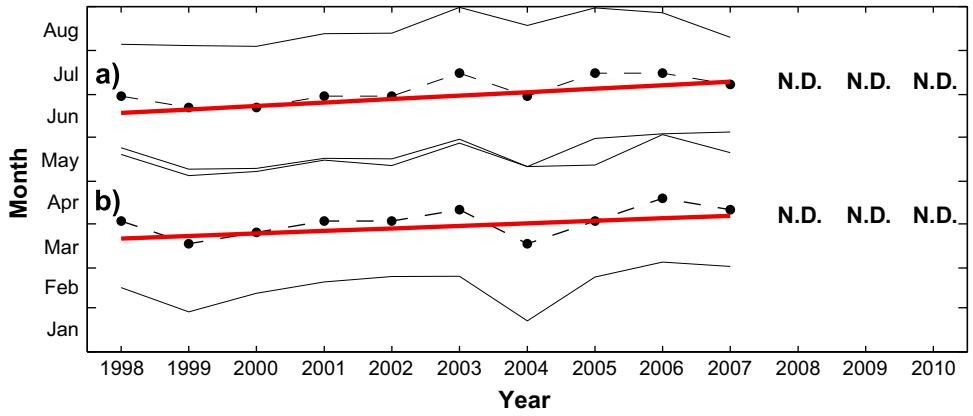

Fig. 8. The phenology of two metrics of the Early Peak seasonal cycle over the study period. Data are medians (black circles), ±1 standard deviation (thin lines) and the least squares linear trend (red lines). The bloom cessation (a) is delaying at 2.44 days yr^{-1} and the bloom initiation (b) is delaying at 1.78 days yr^{-1}. Missing data in 2008, 2009 and 2010 prevented calculation of both of these phenology metrics. (For interpretation of the references to color in this figure legend, the reader is referred to the web version of this article.)

periods with each period quantified by its own metric of phenology. The central tendency metric is effective at isolating timing shifts in longer periods of elevated CHL; this metric uses data from all time steps in its domain. The spring peak metric isolates one particular day when CHL is highest and performs well in identifying specific peaks such as the spring bloom.

The central tendency of the Late Peak summer elevated period (Fig. 7a) is becoming earlier, advancing by 0.63 days yr^{-1} from 1998 to 2007 ($F=23.98$, df=(1, 978), $p<0.01$). We also examine the influence of the 1998 El Niño on this short time series. Without 1998, the slope is 0.70 days yr^{-1} ($F=24.05$, df=(1, 912), $p<0.01$). The variance about this linear slope is small, with 2004 and 2007 as the earliest years, and no specific years anomalously late. These results from the phenology are consistent with the heat-map from the Late Peak seasonal cycle (Fig. 6a). The date of the spring CHL maximum (Fig. 7b) is becoming later, delaying by 1.34 days yr^{-1} from 1998 to 2010 ($F=44.20$, df=(1, 2434), $p<0.01$). Without the El Niño year of 1998, the slope is 1.43 days yr^{-1} ($F=42.77$, df=(1, 2308), $p<0.01$). The interannual variability about the linear trend of this metric shows late years in 2006 and 2007, and early years in 1998 and 2004. The low p-values for all of these slopes suggest the slopes are significantly different than zero. The use of a single date for the spring CHL maximum is less strongly influenced by satellite data outages than the other phenology metrics, so long as the event is unlikely during the period of missing data. Missing data in 2009 occurred during the anticipated date of the spring maximum so this result is excluded. The central tendency requires a more complete time series, thus the missing data from 2008, 2009 and 2010 are problematic and these dates are not included.

Within the Early Peak seasonal group (Fig. 8), the begin and end dates of the annual peak effectively capture the phenology of an important part of the seasonal cycle. Both metrics require a complete time series so the results from 2008, 2009 and 2010 are not shown due to the missing data. The linear trend shows the bloom begin and end dates from 1998 to 2007 are delayed by 1.78 days yr^{-1} ($F=14.08$, df=(1, 1328), $p<0.01$) and 2.44 days yr^{-1} ($F=27.86$, df=(1, 1328), $p<0.01$), respectively, indicating a trend to later seasonality. The difference in slopes also implies that the duration of the bloom is increasing by 0.66 days yr^{-1}. Without the El Niño year of 1998, the bloom begin date is delaying at 2.24 days yr^{-1} ($F=19.40$, df=(1, 1273), $p<0.01$) and the bloom end date is delaying at 2.87 days yr^{-1} ($F=32.97$, df=(1, 1273), $p<0.01$), implying an increase in bloom duration of 0.63 days yr^{-1}. In both metrics, 1998, 2003 and 2006 appear as late years, and 1999 and 2004 as early years, largely consistent with the results from the heat-maps. We could see no consistent connection between the timing of the bloom (Fig. 8) and the spatial extent of this seasonal cycle in the interannual

biogeographic map (Fig. 3), suggesting the phenology shifts are not simply a reflection of changing area.

5. Discussion

5.1. Biogeographic boundaries and seasonal cycles

The biogeographic boundaries defined by climatological seasonal CHL characteristics (Fig. 2) do not show simple latitudinal breaks as is common in previous work (see Section 2.1 for a review) but have some similarities: (1) a discontinuity at Point Conception, between our Late Peak and Early Peak coastal seasonal cycles, (2) the SCB, which contains all four of our seasonal cycles, and is different than the other coastal areas (consistent with findings off the Scripps Pier from Kim et al. (2009)), (3) Cape Mendocino, south of which the Late Peak seasonal cycle becomes very narrow, and (4) Punta Eugenia, south of which the Early Peak seasonal cycle region extends progressively further offshore.

Multivariate clustering of chlorophyll time series by Henson and Thomas (2007) divided the CCS into three regions, with alongshore-oriented boundaries. However, their single coastal region extending over the entire latitudinal range of the CCS resulted from elevated coastal CHL concentrations. Here, normalization by the annual mean removes magnitude from the clustering criteria and shows all four season types are present within 100 km of the coast somewhere over the latitudinal range of the study area.

D'Ortenzio et al. (2012) use multivariate clustering to divide the global ocean into climatological seasonal biogeographic provinces for both the SeaWiFS and CZCS time series separately. Our results provide significantly more detail in the CCS due to our smaller study area, but aspects of our seasonal cycles correspond well in the CCS to their SeaWiFS time series. Specifically, D'Ortenzio et al. (2012) report large areas of a Flat (named Tropical, Cluster #2) and a Summer Min (named Subtropical North, Cluster #3) seasonal cycle in the offshore regions of the CCS. Their coarser spatial resolution, however, means that the Early Peak (named Bloom, Cluster #1), and Late Peak (named Subtropical South, Cluster #4) coastal seasonal cycles are represented by only a few isolated pixels in the CCS, although these do appear in similar locations to where we map them.

To accompany his map of the biogeographic provinces of the global ocean, Longhurst (1995) provides 8 'models' of phytoplankton seasonal cycle types. His third model, titled "Subtropical Nutrient-Limited, Winter-Spring Production Period", corresponds well with the Summer Min seasonal cycle. Similarly, the fourth model from Longhurst (1995), "Tropics" resembles our Flat seasonal cycle. The Late Peak and Early Peak seasonal cycles also correspond well with the eighth model, "Intermittent Production Peaks in Coastal Upwelling Regimes." Geographically, Longhurst (1995) includes the majority of our CCS study area in one biogeographic province characterized as "Intermittent Production Peaks in Coastal Upwelling Regimes" (Model 8). Longhurst (1995) does stress the importance for further work to sub-divide the highly dynamic coastal provinces and in particular the eastern boundary currents for more detailed analysis.

5.2. Physical forcing of climatological biogeography

Each of the four climatological phytoplankton seasonal cycles corresponds well with physical variables that can be mechanistically connected to phytoplankton biomass seasonality. As is typical in sub-tropical and southern temperate regions, climatological wind mixing (not shown) in the area characterized by the Summer Min seasonal cycle is elevated in the winter and fall, and lower during the summer, when heating-induced stratification peaks. In these regions, winter mixing breaks the summer stratification and mixes nutrients into the euphotic zone supporting phytoplankton growth (Strub et al., 1990). Solar heating and reduced wind mixing in the summer inhibit vertical mixing and nutrient flux (Palacios et al., 2004), reducing surface CHL. An alternate hypothesis, but still consistent with seasonal wind forcing, is that fall and winter storms redistribute a summer subsurface CHL maximum into the surface layer where satellites can detect them (Perry et al., 2008). Climatological seasonal cycles of upper mixed layer NO_3 and $Si(OH)_4$ from the eastern station of Line P (west of Vancouver Island) from 1969 to 1981 display a pronounced summer minimum period (Pena and Varela, 2007), which may be due to stratification or possibly a summer subsurface CHL maximum which is depleting the bioavailable nutrients from the euphotic zone.

Geographically, our climatological Summer Min region represents the eastern extent of the much larger oligotrophic gyre in the North Pacific (Yoder and Kennelly, 2003; Thomas et al., 2012b), and suggests that our study area includes the offshore edge of the upwelling influenced CCS. Small areas characterized by the Summer Min seasonal cycle are also present near Punta Eugenia and in the coastal areas along the southern part of the SCB. In this region, the zonal orientation of the coastline, unique bathymetry and shadow of Point Conception from the southward flowing California Current induce weak wind-induced cross shelf transport, strong summer stratification and a recirculation of offshore water close to shore. These hydrographic conditions are likely responsible for a typically offshore seasonal cycle to appear near the coast. Legaard and Thomas (2006) also note differences in the seasonality of both CHL and SST in the SCB compared to regions immediately north and south.

In the northerly coastal region of the CCS (Cape Blanco to Vancouver Island), the climatological upwelling seasonal cycle in alongshore wind forcing drives summer upwelling and fall and winter downwelling (Bakun and Nelson, 1991), matching the CHL seasonality of the Late Peak seasonal cycle (Figs. 2 and 3), and consistent with views from earlier analyses of satellite ocean color data (Hill et al., 1998; Thomas et al., 2001). Along the Washington coast, the transition from the wet winter to the dry summer season (as measured by turbidity) appears associated with the spring peak, whereas coastal upwelling seems to drive the later summer elevated CHL period (Pirhella et al., 2009). Winter light limitation in northerly parts of this region may also influence the local phytoplankton seasonality (Henson and Thomas, 2007).

In the Baja California coastal region, the balance between year-round persistent upwelling-favorable winds and stratification driven by strong solar heating are the primary drivers of phytoplankton seasonality (Espinosa-Carreon et al., 2004). The Early Peak seasonal cycle in CHL increases from November through May, when the upwelling favorable winds (annual maximum in March) work to overcome thermal stratification. Later in the season, stratification limits the supply of nutrients to the euphotic zone and CHL decreases from June through October (Palacios et al., 2004). Similar to the Summer Min seasonal cycle, the Early Peak seasonal cycle also appears climatologically in the SCB (Fig. 2) where the recirculation of the Southern California Eddy causes a discontinuity in the CCS (Checkley and Barth, 2009). Our multivariate clustering analysis also locates the Early Peak seasonal cycle in smaller locations on the British Columbia shelf, outside Juan de Fuca Strait, near Cape Mendocino and San Francisco Bay (Fig. 2), where freshwater discharge or changes in wind forcing due to headlands might shift the phytoplankton seasonal cycle away from similarity with other local areas.

The large latitudinal extent of the Flat seasonal cycle suggests multiple possible explanations for the weak seasonality. South of Point Conception, strong thermal stratification from solar heating

coupled with fewer (or weaker) winter storms keep CHL levels consistently low year-round, typical of global subtropical regions (Longhurst, 1995). From 33°N to 45°N, the Flat seasonal cycle is located just inshore of the region characterized by the Summer Min seasonal cycle (Fig. 2). Seasonal solar heating and wind conditions are likely similar; fall and winter storms move through the region, promoting vertical nutrient flux into the euphotic zone and increasing phytoplankton biomass. In the Flat region, however, offshore advection of coastal upwelling-induced phytoplankton in eddies, filaments and meanders, could elevate summer CHL, keeping the overall seasonality relatively weak year-round. The outer boundary of the region has meandering features characteristic of CCS flow patterns (Hill et al., 1998). North of 45°N, the Flat seasonal cycle extends to the western edge of the study area from the coastal zone (Fig. 2). This geographic region may be more similar to the subarctic North Pacific, where seasonal cycles of CHL are minimal (Parsons and Lalli, 1988). The weak seasonality of the Flat region may also be a product of the climatological averaging. The interannual seasonal biogeography (Fig. 3) and the Simpson Diversity Index (Fig. 5) show elevated interannual variability in the seasonal cycles in this region. However, the persistent presence of the Flat seasonal cycle in the interannual biogeographic analysis (Fig. 3) shows that regions of weak seasonality are present in much of the CCS in every year and not an artifact of multi-year averaging.

5.3. Interannual changes in phytoplankton seasonality and links to physical forcing

With four seasonal cycle types, there are twelve possible changes between the climatology and the actual yearly seasonal cycle at each location, or no change. We provide a view of the interannual shifts between climatology and actual yearly seasonal cycles by quantifying the percent of the study area that makes each shift in each year (Table 1), and mapping the six most dominant shifts in each year (Fig. 9). Table 1 also quantifies the mean percent of the study area that makes each shift over the study period (right-hand column), and the totals for each year, illustrating the degree to which each year differs from the climatology (bottom row). On average, a shift from Summer Min to Flat covers the most area at 11.3%, and the next three most dominant shifts all start from the climatological Flat seasonal cycle (Flat to Summer Min = 10.7%, Flat to Late Peak = 3.8%, and Flat to Early Peak = 5.9%). Not surprisingly, the Flat seasonal cycle, representing the largest area of the study area, and positioned geographically between the productive coastal zones and the offshore region, is involved in the largest shifts between the climatology and the individual years. Geographically, shifts from Flat to Summer Min are more widespread in 1998 and 2007 off Baja California, comprising a large (25.2% and 19.1% of study area, respectively), contiguous region in the southerly portions of the study area (Fig. 9a, black). We investigated the extent to which changes in wind forcing might be consistent with these interannual differences. During these two years in the southern portion of the study area, the seasonally-averaged U^{*3} metric for the winter and fall was larger than usual, indicating that stronger wind events or storms (Fig. 10) potentially reduced the stratification that is typical in this region (climatologically characterized by the Flat seasonal cycle), mixing nutrients into the photic zone, and inducing atypical winter and fall blooms.

In four study years (1999, 2000, 2002 and 2008), relatively large regions (21.0%, 20.0%, 14.2% and 17.6% of the study area, respectively), primarily between ~33°N and 48°N, shifted from Summer Min to Flat (Fig. 9a, gray). Possible mechanistic explanations include: (1) increased summer upwelling which produced higher coastal CHL concentrations that could be transported offshore, (2) weaker fall and winter storms that reduced mixing-induced vertical nutrient flux and decreased the CHL levels in the fall and winter, and (3) stronger than usual wind stress curl in the summer, which shoaled the thermocline offshore and delivered nutrients to the photic zone, producing local blooms. The wind data (not shown) support the first hypothesis for 1999, 2002 and 2008 and the second hypothesis for 2000. Trends in the summer wind stress curl in this region in our data are not evident in these years due to large variability.

Over our study period, interannual variability in seasonal geography appears most strongly associated with the 1998–1999 El Niño and subsequent La Niña conditions. The largest annual total area of seasonality shifts (Table 1, bottom row) occurred in 1998 and 1999 (45.0% and 51.0% of the study area, respectively). An expansion offshore of the Flat seasonal cycle into the climatological Summer Min region in 1998 (25.2% of study area) and the opposite shift in 1999 (21.0% of study area) comprised much of these totals. In addition, the Late Peak and Early Peak seasonal cycles contracted in 1998, and the Flat seasonal cycle expanded toward shore. The opposite occurred in 1999. Quantitatively, 2.6%

Table 1
Percent of the study area that shifts from the climatological seasonal cycle (Fig. 2) in each year (Fig. 3); SM = Summer Min, LP = Late Peak, EP = Early Peak, FL = Flat.

	1998	1999	2000	2001	2002	2003	2004	2005	2006	2007	2008	2009	2010	Avg[a]
Summer Min to														
LP	0.1	0.3	0.0	0.1	0.4	1.5	0.0	0.4	0.3	0.1	0.1	0.0	0.1	0.3
EP	0.2	0.9	0.4	2.4	2.5	0.9	0.4	2.0	0.7	2.5	1.6	0.5	1.3	1.3
FL	10.4	21.0	20.0	5.4	14.2	7.3	7.9	10.7	11.5	6.5	17.6	7.4	6.9	11.3
Late Peak to														
SM	0.2	0.0	0.0	0.0	0.0	0.3	0.4	0.1	0.2	0.0	0.0	0.0	0.0	0.1
EP	0.9	1.2	0.9	1.2	1.9	2.1	2.8	0.2	1.7	1.8	1.4	0.4	0.4	1.3
FL	2.6	0.5	0.9	1.0	0.7	1.1	1.3	2.5	1.6	1.8	0.4	2.2	0.9	1.3
Early Peak to														
SM	2.3	1.1	0.1	1.1	0.1	0.0	0.1	0.0	1.3	0.6	0.0	0.1	0.1	0.5
LP	0.1	0.1	0.2	0.6	0.5	1.2	0.2	0.8	0.2	0.2	0.1	0.2	1.1	0.4
FL	0.8	0.1	0.0	0.6	0.1	0.0	0.2	0.2	0.0	0.7	0.0	0.0	1.6	0.3
Flat to														
SM	25.2	12.4	2.8	9.1	12.1	7.3	11.4	2.9	9.1	19.1	6.1	13.9	8.2	10.7
LP	0.9	5.3	2.5	4.0	3.0	4.9	1.9	8.7	4.8	2.5	4.1	1.7	5.0	3.8
EP	1.5	8.0	7.6	6.4	7.2	9.7	5.7	3.5	5.8	4.4	11.2	3.1	2.9	5.9
Annual total	45.0	51.0	35.5	31.8	42.5	36.3	32.4	31.8	37.1	40.0	42.6	29.7	28.5	

[a] The average for each type of shift is the mean over the 13-year study period.

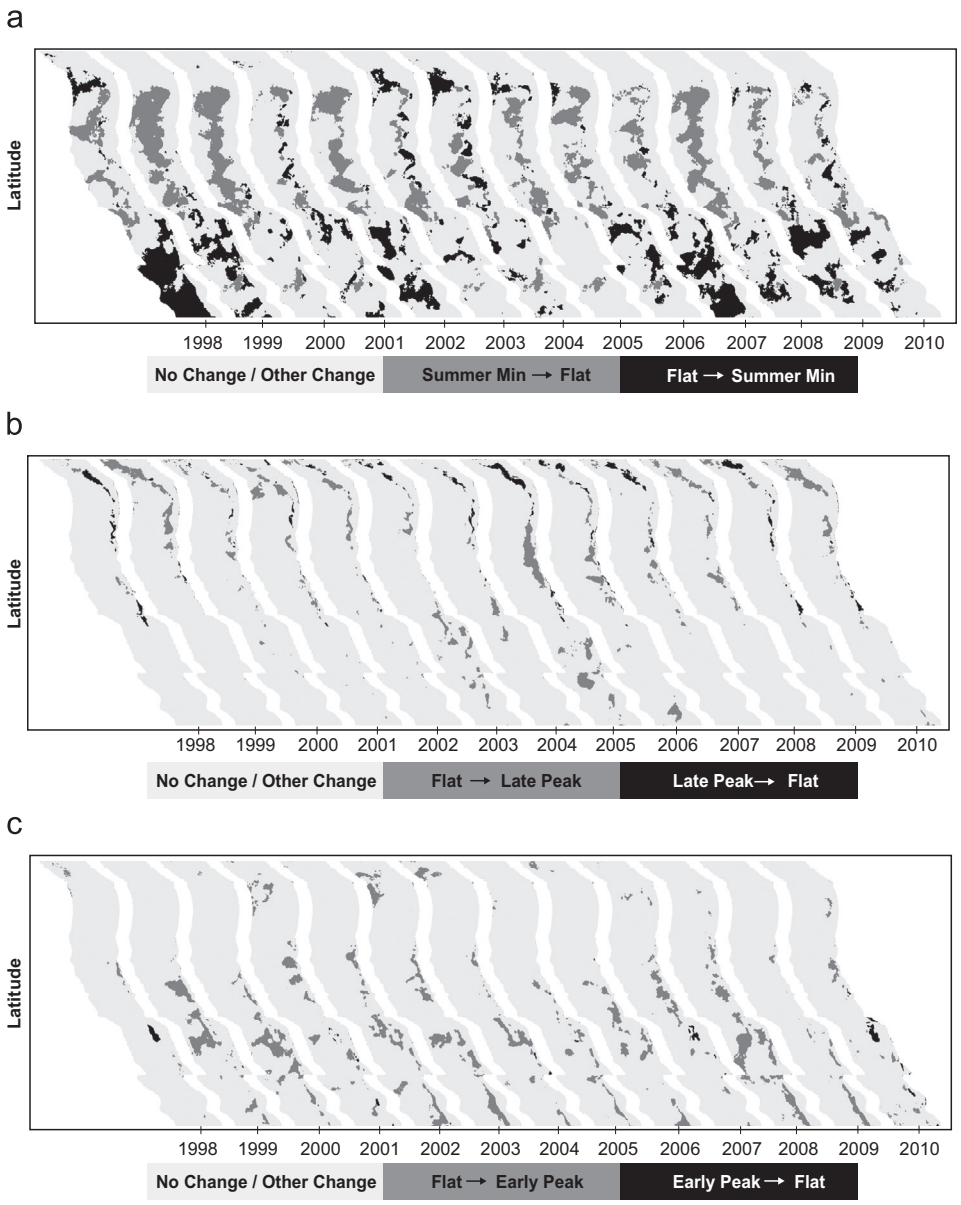

Fig. 9. Location-specific changes in the cluster assignments from the climatological seasonal cycle to the interannual seasonal cycle for six dominant changes. (a) Shifts between the Summer Min and Flat seasonal cycles. (b) Shifts between the Flat and Late Peak seasonal cycles. (c) Shifts between the Flat and Early Peak seasonal cycles.

of the study area shifted in 1998 from a climatological Late Peak seasonal cycle to the Flat seasonal cycle (Fig. 9b, black), the maximum for the 13 year study period (Table 1). In 1999, the same shift occurred in 0.5% of the study area, the minimum over the study period. In contrast, in 1998, only 0.9% of the study area shifted from the Flat to the Late Peak seasonal cycles (Fig. 9b, gray), representing the minimum, compared to 5.3% in 1999, the study period's maximum. Similarly, in 1998, 1.5% of the study area made the switch from Flat to Early Peak (Fig. 9c, gray), the minimum for the 13 years and in 1999, the La Niña year, 8.0% switched, one of the top three years. The opposite shift, from Early Peak to Flat (Fig. 9c, black), occurred in only 0.8% of the study area in 1998, but was still larger than the 0.1% that shifted in 1999. These shifts are consistent with the canonical view of ENSO impacts on the CCS: a deeper, nutrient-poor upper layer, stronger stratification, weaker upwelling and an expansion of more oligotrophic conditions (*e.g.* Kahru and Mitchell, 2000; Mackas, 2006).

In 2005, the delayed upwelling season caused a later than usual phytoplankton bloom off the Oregon and northern and central California coasts (Thomas and Brickley, 2006). Our analysis shows the Late Peak seasonal cycle area had a net expansion of 7.2% in 2005 (Fig. 9b, gray) to encompass a wide area off these coastlines, the largest such change in the data set.

The overall trend over the study period in regions characterized by the Late Peak seasonal cycle is a delaying spring CHL maximum and an advancing summer central tendency (Fig. 7). Together, these results imply that the season of elevated phytoplankton biomass is delaying and shortening over northern coastal upwelling regions of our study area. This trend is consistent with results from Bograd et al. (2009) that demonstrate a shift of upwelling-favorable winds in the northern CCS to later and shorter seasons from 1967 to 2007.

Study period trends for the Early Peak CHL seasonal cycle (southern coastal CCS) show it delaying and becoming longer (Fig. 8). Bograd et al. (2009) reports a lengthening of the upwelling season in the southern CCS but not a delay in the onset of the upwelling winds. One possible explanation for the delaying of the bloom in the Early Peak seasonal cycle is increased winter stratification due to warmer winters, which would require more cumulative upwelling to shoal isopycnals, and thus a later biomass

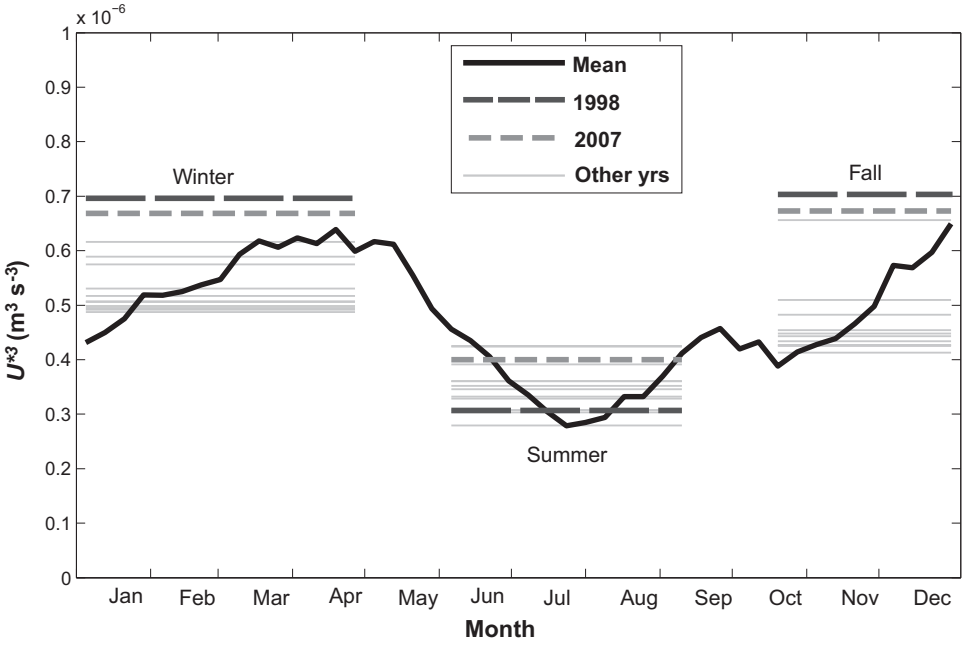

Fig. 10. The wind mixing power (U^{*3}) offshore of Baja California. The climatology is shown as the bold solid line. The horizontal bars indicate the seasonally-averaged wind mixing power in individual study years, with 1998 and 2007 highlighted with dashed lines.

increase. Consistent with this hypothesis, Palacios et al. (2004) report a strengthening of stratification and heat content from 1950 to 1993 at a coastal site at 32°N, 118°W, located in the northern tip of the area characterized by the climatological Early Peak seasonal cycle. However, trends toward enhanced winter stratification cannot explain the trend toward a delay in the end of the seasonal CHL bloom, a result that requires more detailed analysis of possible mechanistic controls.

6. Summary and conclusions

Classification of seasonal cycles evident in 13 years of SeaWiFS satellite CHL over the California Current finds four dominant temporal patterns: two with spring-summer maxima, one with a summer minimum and a fourth with very weak seasonality. In the climatology, these map to four distinct regions: two coastal (northern and southern) representing coastal upwelling regions, one offshore, and one between these that extends the entire latitudinal range of the CCS. Strong interannual variability in the spatial structure of these regions validates the argument that static boundaries in the ocean may be misleading and do not necessarily reflect the conditions at any given period in time. Quantification of the frequency with which locations shift seasonal cycles shows that areas along Vancouver Island, Washington and Oregon coasts, farthest offshore of the California coast, and near the southern Baja California coast are most stable on an interannual basis. Regions of most frequent changes in seasonal cycle shapes are the SCB, the northern and central California coastal upwelling areas and the seaward margin of the upwelling region along the Baja California coast.

Clustering analysis provides an effective technique to dividing the temporally varying structure of phytoplankton seasonality across the CCS. A novel approach to assessing interannual variability in the biogeography treats each individual seasonal cycle as an independent vector and clusters all 13 years of data with a single clustering operation. Different clusters might arise if single years were treated individually. The four clusters defined in the climatology are not necessarily optimal in any one year but provide a consistent framework with which to compare all 13 years. Multivariate clustering has subjective aspects, and other clustering procedures might find more, fewer, or different groupings of seasonal cycles, depending on the goals and objectives of the study. Here, our goal is to provide a view of interannual variability in the spatial geography of the primary seasonal cycle shapes present across the CCS.

The phenology results indicate that although coherent delays in the spring are evident in the two seasonal cycle shapes that characterize the CCS coastal upwelling zones, trends in the latter part of the seasonality are not similar between these seasonal cycle types. The phenology of the Late Peak seasonal cycle is delaying and becoming shorter, consistent with shifts in the seasonal cycle of upwelling observed by other authors. The spring maximum in the Early Peak seasonal cycle is delaying and increasing in duration, the latter of which is also consistent with trends in upwelling. The impacts of these changes on the ecosystem are not known, but provide clear scenarios to examine with either coupled biophysical or trophic models.

Though shifts in the timing of individual phytoplankton seasonal cycles in the CCS are evident, trends in the biogeographic ranges of the seasonal cycles are not evident in our results in contrast to reports for open ocean oligotrophic regions (Irwin and Oliver, 2009), zooplankton species' ranges (Beaugrand et al., 2002) and the mean temperature of catch in fisheries (Cheung et al., 2013). However, it is not clear whether latitudinal shifts in response to a changing climate should be expected in an upwelling zone. The view presented here is of regions partitioned by the seasonal cycle shape, which might be less susceptible to temperature trends than regions defined by characteristics such as individual species' ranges. Furthermore, 13 years of data (and ten for some of the phenology metrics), is short for quantifying any trend attributable to global warming, with some results showing that 40 years of data is required (Henson et al., 2010).

Acknowledgments

We thank the NASA Ocean Color Biology group at Goddard Space Flight Center and the NOAA National Climate Data Center for

making the SeaWiFS and Blended Sea Winds data freely available as well as Ryan Weatherbee and Kerstin Cullen in the Satellite Oceanography Data Lab at the University of Maine for their help and consultation. We thank all the co-PIs of our GLOBEC synthesis project for stimulating interactions, especially E. Di Lorenzo of Georgia Tech for leading the POBEX project. This work was funded by NSF grants OCE-0815051 and OCE-0814413, and the NASA Earth and Space Science Fellowship grant no. NNX12AP26H. GLOBEC contribution no. 747.

References

Bane, J.M., Spitz, Y.H., Letelier, R.M., Peterson, W.T., 2007. Jet stream intraseasonal oscillations drive dominant ecosystem variations in Oregon's summertime coastal upwelling system. Proc. Nat. Acad. Sci. U.S.A. 104 (33), 13262–13267, http://dx.doi.org/10.1073/pnas.0700926104.

Bakun, A., 1990. Global climate change and intensification of coastal ocean upwelling. Science 247 (4939), 198–201.

Bakun, A., Nelson, C.S., 1991. The seasonal cycle of wind-stress curl in subtropical eastern boundary current regions. J. Phys. Oceanogr. 21, 1815–1834.

Barth, J.A., Menge, B.A., Lubchenco, J., Chan, F., Bane, J.M., Kirincich, A.R., McManus, M.A., Nielsen, K.J., Pierce, S.D., Washburn, L., 2007. Delayed upwelling alters nearshore coastal ocean ecosystems in the northern California current. Proc. Nat. Acad. Sci. U.S.A. 104 (10), 3719–3724, http://dx.doi.org/10.1073/pnas.0700462104.

Beaugrand, G., Reid, P.C., Ibañez, F., Lindley, J.A., Edwards, M., 2002. Reorganization of North Atlantic marine copepod biodiversity and climate. Science 296 (5573), 1692–1694.

Black, B.A., Schroeder, I.D., Sydeman, W.J., Bograd, S.J., Wells, B.K., Schwing, F.B., 2011. Winter and summer upwelling modes and their biological importance in the California current ecosystem. Global Change Biol. 17, 2536–2545, http://dx.doi.org/10.1111/j.1365-2486.2011.02422.x.

Bograd, S.J., Schroeder, I.D., Sarkar, N., Qiu, X., Sydeman, W.J., Schwing, F.B., 2009. Phenology of coastal upwelling in the California current. Geophys. Res. Lett. 36, L01602.

Brander, K.M., Dickson, R.R., Shepherd, J.G., 2001. Modelling the timing of plankton production and its effect on recruitment of cod (*Gadus morhua*). ICES J. Mar. Sci. 58, 962–966, http://dx.doi.org/10.1006/jmsc.2001.1086.

Brody, S.R., Lozier, M.S., Dunne, J.P., 2013. A comparison of methods to determine phytoplankton bloom initiation. J. Geophys. Res. 118, 2345–2357, http://dx.doi.org/10.1002/jgrc.20167.

Campbell, J.W., 1995. The lognormal distribution as a model for bio-optical variability in the sea. J. Geophys. Res. 100, 13237–13254.

Checkley Jr., D.M., Barth, J.A., 2009. Patterns and processes in the California Current System. Prog. Oceanogr. 83, 49–64.

Chenillat, F., Rivière, P., Capet, X., Di Lorenzo, E., Blanke, B., 2012. North Pacific Gyre Oscillation modulates seasonal timing and ecosystem functioning in the California Current upwelling system. Geophys. Res. Lett. 39, L01606, http://dx.doi.org/10.1029/2011GL049966.

Cheung, W.W. L., Watson, R., Pauly, D., 2013. Signature of ocean warming in global fisheries catch. Nature 497, 365–368, http://dx.doi.org/10.1038/nature12156.

Cushing, D.H., 1990. Plankton production and year-class strength in fish populations: an update of the match/mismatch hypothesis. Adv. Mar. Biol. 26, 249–293.

Denman, K.L., Powell, T.M., 1984. Effects of physical processes on planktonic ecosystems in the coastal ocean. Oceanogr. Mar. Biol. 22, 125–168.

Denman, K.L., Abbott, M., 1988. Time evolution of surface chlorophyll patterns from cross-spectrum analysis of satellite color images. J. Geophys. Res. 93 (C6), 6789–6798.

Devred, E., Sathyendranath, S., Platt, T., 2007. Delineation of ecological provinces using ocean colour radiometry. Mar. Ecol. Prog. Ser. 346, 1–13.

Di Lorenzo, E., Ohman, M.D., 2012. A double-integration hypothesis to explain ocean ecosystem response to climate forcing. Proc. Nat. Acad. Sci. U.S.A. 110 (7), 2496–2499, http://dx.doi.org/10.1073/pnas.1218022110.

Doney, S.C., Ruckelshaus, M., Duffy, J.E., Barry, J.P., Chan, F., English, C.A., Galindo, H.M., Grebmeier, J.M., Hollowed, A.B., Knowlton, N., Polovina, J., Rabalais, N.N., Sydeman, W.J., Talley, L.D., 2012. Climate change impacts on marine ecosystems. Annu. Rev. Mar. Sci. 4, 11–37.

Dorman, J.G., Powell, T.M., Sydeman, W.J., Bograd, S.J., 2011. Advection and starvation cause krill (*Euphausia pacifica*) decreases in 2005 Northern California coastal populations: implications from a model study. Geophys. Res. Lett. 38, L04605, http://dx.doi.org/10.1029/2010GL046245.

D'Ortenzio, F., Ribera d'Alcalà, M., 2009. On the trophic regimes of the Mediterranean Sea: a satellite analysis. Biogeosciences 6, 139–148.

D'Ortenzio, F., Antoine, D., Martinez, E., d'Alcalà, M.R., 2012. Phenological changes of oceanic phytoplankton in the 1980s and 2000s as revealed by remotely sensed ocean-color observations. Global Biogeochem. Cycles 26, GB4003.

Edwards, M., Richardson, A.J., 2004. Impact of climate change on marine pelagic phenology and trophic mismatch. Nature 430, 881–883.

Espinosa-Carreon, T.L., Strub, P.T., Beier, E., Ocampo-Torres, F., Gaxiola-Castro, G., 2004. Seasonal and interannual variability of satellite-derived chlorophyll pigment, surface height, and temperature off Baja California. J. Geophys. Res. 109, C03039, http://dx.doi.org/10.1029/2003JC002105.

Fuentes-Yaco, C., Koeller, P.A., Sathyendranath, S., Platt, T., 2007. Shrimp (*Pandalus borealis*) growth and timing of the spring phytoplankton bloom on the Newfoundland–Labrador Shelf. Fish. Oceanogr. 16 (2), 116–129.

GLOBEC (1991). Eastern Boundary Current Program, Report on Climate Change and the California Current Ecosystem, Report #7. Mackas D., Strub T., and Hunter J. (Eds.).

Greve, W., Prinage, S., Zidowitz, H., Nast, J., Reiners, F., 2005. On the phenology of North Sea ichthyoplankton. ICES J. Mar. Sci. 62, 1216–1223.

Haury, L.R., McGowan, J.A., Wiebe, P.H., 1978. In: Steele, J.H. (Ed.), Patterns and processes in the time-space scales of plankton. In: Spatial Patterns in Plankton Communities. Plenum Press, New York, NY., pp. 277–327.

Henson, S.A., Thomas, A.C., 2007. Interannual variability in timing of bloom initiation in the California Current System. J. Geophys. Res. 112, C08007.

Henson, S.A., Robinson, I., Allen, J.T., Waniek, J.J., 2006. Effect of meteorological conditions on interannual variability in timing and magnitude of the spring bloom in the Irminger Basin, North Atlantic. Deep Sea Res. Part I 53, 1601–1615, http://dx.doi.org/10.1016/j.dsr.2006.07.009.

Henson, S.A., Sarmiento, J.L., Dunne, J.P., Bopp, L., Lima, I., Doney, S.C., John, J., Beaulieu, C., 2010. Detection of anthropogenic climate change in satellite records of ocean chlorophyll and productivity. Biogeosciences 7, 621–640.

Hickey, B., 1989. Patterns and processes of circulation over the Washington continental shelf and slope. In: Landy, M., Hickey, B. (Eds.), Coastal Oceanography of Washington and Oregon. Elsevier Science, Amsterdam, pp. 41–109.

Hill, A.E., Hickey, B.M., Shillington, F.A., Strub, P.T., Brink, K.H., Barton, E.D., Thomas, A.C., 1998. Eastern ocean boundaries: coastal segment. In: Robinson, A., Brink, K. (Eds.), The Sea, Vol. 11. John Wiley and Sons, Inc., New Jersey, pp. 29–67.

Hjort, J. (1914), Fluctuations in the Great Fisheries of Northern Europe, Rapports et Procès-Verbaux, Conseil Permament International Pour l'Exploration de la Mer, Volume XX.

Holt, C.A., Mantua, N., 2009. Defining spring transition: regional indices for the California Current System. Mar. Ecol. Prog. Ser. 393, 285–299.

IPCC, 2007. Climate Change 2007: Synthesis Report. Contribution of Working Groups I, II and III to the Fourth Assessment Report of the Intergovernmental Panel on Climate Change. In: Pachauri, R.K., Reisinger, A. (Eds.), IPCC, Geneva, Switzerland, p. 104 (Core Writing Team).

Irwin, A.J., Oliver, M.J., 2009. Are ocean deserts getting larger? Geophys. Res. Lett. 36, L18909.

Ji, R., Edwards, M., Mackas, D.L., Runge, J.A., Thomas, A.C., 2010. Marine plankton phenology and life history in a changing climate: current research and future directions. J. Plankton Res. 32 (10), 1355–1368.

Kahru, M., Mitchell, B.G., 1999. Empirical chlorophyll algorithm and preliminary SeaWiFS validation for the California Current. Int. J. Remote Sens. 20 (17), 3423–3429.

Kahru, M., Mitchell, B.G., 2000. Influence of the 1997–1998 on the surface chlorophyll in the California Current. Geophys. Res. Lett. 27 (18), 2937–2940.

Kahru, M., Mitchell, B.G., 2001. Seasonal and nonseasonal variability of satellite-derived chlorophyll and colored dissolved organic matter concentration in the California Current. J. Geophys. Res. 06 (C2), 2517–2529.

Kahru, M., Kudela, R., Manzano-Sarabia, M., Mitchell, B.G., 2009. Trends in primary production in the California Current detected with satellite data. J. Geophys. Res. 114, C02004.

Kahru, M., Brotas, V., Manzano-Sarabia, M., Mitchell, B.G., 2011. Are phytoplankton blooms occurring earlier in the Arctic? Global Change Biol. 17, 1733–1739, http://dx.doi.org/10.1111/j.1365-2486.2010.02312.x.

Kim, H., Miller, A.J., McGowan, J., Carter, M.L., 2009. Coastal phytoplankton blooms in the Southern California Bight. Prog. Oceanogr. 82, 137–147.

Kirby, R.R., Beaugrand, G., 2009. Trophic amplification of climate warming. Proc. R. Soc. London, Ser. B 276, 4095–4103.

Koeller, P., Fuentes-Yaco, C., Platt, T., Sathyendranath, S., Richards, A., Ouellet, P., Orr, D., Skúladóttir, U., Wieland, K., Savard, L., Aschan, M., 2009. Basin-scale coherence in phenology of shrimps and phytoplankton in the North Atlantic Ocean. Science 324, 791–793.

Kosro, P.M., Peterson, W.T., Hickey, B.M., Shearman, R. K, Pierce, S.D., 2006. Physical versus biological spring transition: 2005. Geophys. Res. Lett. 33, L33S03.

Legaard, K.R., Thomas, A.C., 2006. Spatial patterns in seasonal and interannual variability of chlorophyll and sea surface temperature in the California Current. J. Geophys. Res. 111, C06032, http://dx.doi.org/10.1029/2005JC003282.

Longhurst, A., 1995. Seasonal cycles of pelagic production and consumption. Prog. Oceanogr. 36, 77–167.

Longhurst, A., 2007. Ecological Geography of the Sea. Academic Press, Burlington, MA.

Mackas, D.L., Denman, K.L., Abbott, M.R., 1985. Plankton patchiness: biology in the physical vernacular. Bull. Mar. Sci. 37 (2), 652–674.

Mackas, D.L., 2006. Interdisciplinary oceanography of the western North American continental margin: Vancouver Island to the tip of Baja California. In: Robinson, A., Brink, K. (Eds.), The Sea, Vol. 12. John Wiley and Sons, Inc., New Jersey, pp. 441–501.

Mann, K.H., Lazier, J.R. N., 2006. Dynamics of Marine Ecosystems: Biological-Physical Interactions in the Oceans. Blackwell Scientific Productions, Oxford.

Manly, B., 2004. Multivariate Statistical Methods: A Primer, third ed. Chapman & Hall/CRC Press, Florida.

Oliver, M.J., Irwin, A.J., 2008. Objective global ocean biogeographic provinces. Geophys. Res. Lett. 35, L15601.

Okamoto, S., Hirawake, T., Saitoh, S.-I., 2010. Interannual variability in the magnitude and timing of the spring bloom in the Oyashio region. Deep Sea Res. Part II 57, 1608–1617.

O'Reilly, J., Maritorena, S., Mitchell, B.G., Siegel, D.A., Carder, K.L., Kahru, M., Garver, S.A., McClain, C.R., 1998. Ocean color algorithms for SeaWiFS. J. Geophys. Res. 103, 24937–24953.
Palacios, D.M., Bograd, S.J., Mendelssohn, R., Schwing, F.B., 2004. Long-term and seasonal trends in stratification in the California Current, 1950–1993. J. Geophys. Res. 109, C10016, http://dx.doi.org/10.1029/2004JC002380.
Parmesan, C., 2006. Ecological and evolutionary responses to recent climate change. Annu. Rev. Ecol. Evol. Syst. 37, 637–669.
Parsons, T.R., Lalli, C.M., 1988. Comparative oceanic ecology of the plankton communities of the subarctic Atlantic and Pacific oceans. Oceanogr. Mar. Biol. 26, 317–359.
Pena, M.A., Varela, D.E., 2007. Seasonal and interannual variability in phytoplankton and nutrient dynamics along Line P in the NE subarctic Pacific. Prog. Oceanogr. 75, 200–222, http://dx.doi.org/10.1016/j.pocean.2007.08.009.
Perry, M.J., Sackmann, B.S., Eriksen, C.C., Lee, C.M., 2008. Seaglider observations of blooms and subsurface chlorophyll maxima off the Washington coast. Limnol. Oceanogr. 53 (5, part 2), 2169–2179.
Pielou, E.C., 1977. Mathematical Ecology. John Wiley & Sons, New York, NY.
Pielou, E.C., 1984. The Interpretation of Ecological Data. John Wiley & Sons, New York, NY.
Pierce, S.D., Barth, J.A., Thomas, R.E., Fleischer, G.W., 2006. Anomalously warm July 2005 in the Northern California Current: historical context and the significance of cumulative wind stress. Geophys. Res. Lett. 33, L22S04, http://dx.doi.org/10.1029/2006GL027149.
Pirhella, D., Ransibrahmanakul, V., Clark, R., 2009. An oceanographic characterization of the Olympic Coast National Marine Sanctuary and Pacific Northwest: interpretive summary of ocean climate and regional processes through satellite remote sensing, NOAA Technical Memorandum. NOS NCCOS, 90.
Platt, T., Sathyendranath, S., 2008. Ecological indicators for the pelagic zone of the ocean from remote sensing. Remote Sens. Environ. 112, 3426–3436.
Platt, T., Caverhill, C., Sathyendranath, S., 1991. Basin-scale estimates of oceanic primary production from remote sensing. J. Geophys. Res. 96 (C8), 15147–15159.
Racault, M. -F., Le Quéré, C., Buitenhuis, E., Sathyendranath, S., Platt, T., 2012. Phytoplankton phenology in the global ocean. Ecol. Indic. 14, 152–163.
Rousseeuw, P.J., 1987. Silhouettes: a graphical aid to the interpretation of cluster analysis. J. Comput. Appl. Math. 20, 53–65.
Richardson, A.J., 2008. In hot water: zooplankton and climate change. ICES J. Mar. Sci. 65, 279–295.
Richardson, A.J., 2009. Plankton and climate. In: Encyclopedia of Ocean Sciences. Academic Press, New York.
Schwing, F.B., Bond, N.A., Bograd, S.J., Mitchell, T., Alexander, M.A., Mantua, N., 2006. Delayed coastal upwelling along the U.S. West Coast in 2005: a historical perspective. Geophys. Res. Lett. 33, L22S01.
Siegal, D.A., Doney, S.C., Yoder, J.A., 2002. The North Atlantic spring phytoplankton bloom and Sverdrup's critical depth hypothesis. Science 296, 730, http://dx.doi.org/10.1126/science.1069174.
Simpson, E.H., 1949. Measurement of diversity. Nature 163, 688.
Sokal, R.R., Rohlf, F.J., 1995. Biometry: The Principles and Practice of Statistics in Biological Research, third ed. W.H. Freeman and Company, New York, NY.
Sydeman, W.J., Bradley, R.W., Warzybok, P., Abraham, C.L., Jahncke, J., Hyrenbach, K.D., Kousky, V., Hipfner, J.M., Ohman, M.D., 2006. Planktivorous auklet *Ptychoramphus aleuticus* responses to ocean climate, 2005: unusual atmospheric blocking? Geophys. Res. Lett. 33, L22S09.
Strub, P.T., Allen, J.S., Huyer, A., Smith, R.L., 1987. Large-scale structure of the spring transition in the coastal ocean off western North America. J. Geophys. Res. 92, 1527–1544.
Strub, P.T., James, C., Thomas, A.C., Abbott, M.R., 1990. Seasonal and nonseasonal variability of satellite-derived surface pigment concentration in the California Current. J. Geophys. Res. 95 (11), 501–511.
Taylor, J.R., Allen, J.I., Clark, P.A., 2002. Extraction of a weak climatic signal by an ecosystem. Nature 416, 629–632.
Thomalla, S.J., Fauchereau, N., Swart, S., Moneiro, P.M. S., 2011. Regional scale characteristics of the seasonal cycle of chlorophyll in the Southern Ocean. Biogeosciences 8, 2849–2866, http://dx.doi.org/10.5194/bg-8-2849-2011.
Thomas, A.C., Brickley, P., 2006. Satellite measurements of chlorophyll distribution during spring 2005 in the California Current. Geophys. Res. Lett. 33, L22S05, http://dx.doi.org/10.1029/2006GL026588.
Thomas, A.C., Strub, P.T., 1989. Interannual variability in phytoplankton pigment distribution during the spring transition along the west coast of North America. J. Geophys. Res. 94 (C12), 18095–18117.
Thomas, A.C., Strub, P.T., 2001. Cross-shelf phytoplankton pigment variability in the California Current. Cont. Shelf Res. 21, 1157–1190.
Thomas, A.C., Carr, M., Strub, P.T., 2001. Chlorophyll variability in eastern boundary currents. Geophys. Res. Lett. 28 (18), 3421–3424.
Thomas, A.C., Strub, P.T., Brickley, P., 2003. Anomalous satellite-measured chlorophyll concentrations in the northern California Current in 2001–2002. Geophys. Res. Lett. 30 (15), 8022, http://dx.doi.org/10.1029/2003GL017409.
Thomas, A.C., Strub, P.T., Weatherbee, R.A., James, C., 2012b. Satellite views of Pacific chlorophyll variability: comparisons to physical variability, local versus non-local influences and links to climate indices. Deep Sea Res. Part II 77–80, 99–116.
Thomas, A.C., Mendelssohn, R., Weatherbee, R., 2013. Background trends in California Current surface chlorophyll concentrations: a state-space view. J. Geophys. Res. 118, 5296–5311, http://dx.doi.org/10.1002/jgrc.20365.
Thomas, M.K., Kremer, C.T., Klausmeier, C.A., Litchman, E., 2012a. A global pattern of thermal adaptation in marine phytoplankton. Science 338, 1085–1088, http://dx.doi.org/10.1126/science.1224836.
Vantrepotte, V., Mélin, F., 2009. Temporal variability of 10-year global SeaWiFS time-series of phytoplankton chlorophyll *a* concentration. ICES J. Mar. Sci. 66, 1547–1556.
Walther, G. -R., Post, E., Convey, P., Menzel, A., Parmesan, C., Beebee, T.J. C., Fromentin, J. -M., Hoegh-Guldberg, O., Bairlein, F., 2002. Ecological responses to recent climate change. Nature 416, 389–395.
Ware, D.M., Thomson, R.E., 2005. Bottom-up ecosystem trophic dynamics determine fish production in the Northeast Pacific. Science 308 (5726), 1280–1284.
Yang, L.H., Rudolf, V.H.W., 2010. Phenology, ontogeny and the effects of climate change on the timing of species interactions. Ecol. Lett. 13, 1–10.
Yelland, M., Taylor, P.K., 1996. Wind stress measurements from the open ocean. J. Phys. Oceanogr. 26, 541–558.
Yoder, J.A., Kennelly, M.A., 2003. Seasonal and ENSO variability in global ocean phytoplankton chlorophyll derived from 4 years of SeaWiFS measurements. Global Biogeochem. Cycles 17 (4), 1112, http://dx.doi.org/10.1029/2002GB001942.
Yoo, S., Batchelder, H.P., Peterson, W.T., Sydeman, W.J., 2008. Seasonal, interannual and event scale variation in North Pacific ecosystems. Prog. Oceanogr. 77, 155–181, http://dx.doi.org/10.1016/j.pocean.2008.03.013.
Zhang, H. –M., Bates, J.J., Reynolds, R.W., 2006. Assessment of composite global sampling: sea surface wind speed. Geophys. Res. Lett. 33, L17714, http://dx.doi.org/10.1029/2006GL027086.